Preparation of three-dimensional fiber-network chitosan films for the efficient treatment of uranium-contaminated effluents

Ying Wang, Yanxiang Li, Lei Li, Fangong Kong, Song Lin, Zaiqian Wang and Wangliang Li

ABSTRACT

A fiber-network chitosan film with three-dimensional interconnected structure was prepared in an alkali/urea solution and regenerated from an ethanol/water coagulation solution. The surface morphology and structure were characterized by scanning electron microscopy (SEM), X-ray diffraction (XRD), N_2 adsorption-desorption, attenuated total reflection Fourier transform infrared spectroscopy (ATR-FTIR) and X-ray photoelectron spectroscopy (XPS). Batch adsorption for uranium U(VI) was conducted to investigate the effects of pH, contact time and initial uranium concentration on adsorption capacity. The adsorption of CS-80% was in good agreement with the pseudo-second-order kinetic model and Langmuir isotherm model. The three-dimensional interconnected structure provided more active sites and favored the diffusion of uranium solute, and therefore enhanced the adsorption capacity. The maximum adsorption capacity at pH 5 was 196.735 mg/g. The adsorption mechanism was attributed to chelation and coordination of uranium with -NH_2 and -OH groups on chitosan molecules.

Key words | adsorption, chitosan, fiber network, film, uranium

Ying Wang
Yanxiang Li
Lei Li
Wangliang Li (corresponding author)
Key Laboratory of Green Process and Engineering,
Institute of Process Engineering,
Chinese Academy of Sciences,
Beijing 100190, China
E-mail: *wlli@ipe.ac.cn*

Ying Wang
University of Chinese Academy of Sciences,
Beijing 100049, China

Fangong Kong
Key Laboratory of Pulp and Paper Science & Technology of Ministry of Education/Shandong Province,
Qilu University of Technology,
Jinan 250353, China

Song Lin
Zaiqian Wang
Guizhou Water Fuquan Co., Ltd,
Guiyang 550500, China

INTRODUCTION

As one of the most efficient energy sources, nuclear energy accounts for approximately 13% of the world's electricity generation (Liu *et al.* 2017). Uranium is the major resource for nuclear energy and is expected to play an important role in energy in the near future, so the demand for uranium is increasing. However, the exploitation and processing of uranium resources are accompanied by uranium contamination. Toxic uranium pollutants bring high risks to the environment and human health, especially due to their characteristics of persistence and bioaccumulativity (Kurttio *et al.* 2005).

In order to effectively remove uranium pollution, various technologies have been applied to separate and recycle uranyl ions U(VI) from aqueous solutions, including electrochemical methods (Liu *et al.* 2017), chemical precipitation, ion exchange (Tavakoli *et al.* 2013), film separation (Zhou *et al.* 2014), extraction (Amaral & Morais 2010) and adsorption (Wang *et al.* 2018), etc. Among these methods, adsorption is regarded as one of the most promising because of its low cost and high efficiency in the treatment of uranyl ions in industrial wastewater. Many kinds of adsorbents have been used for U(VI) adsorption, including clay minerals (Wang *et al.* 2010), modified silica (Dolatyari *et al.* 2016), activated carbon (Chiramba *et al.* 2019), graphene oxide, etc. However, these adsorbents tend to be released into the wastewater and difficult to recycle, which undoubtedly brings secondary pollution to the environment.

Chitosan is the second most abundant natural polysaccharide in the world. It is a biocompatible, biodegradable, biorenewable and non-toxic biopolymer, which has demonstrated a high adsorption capacity for heavy metal ions because of the presence of functional groups like hydroxyl (-OH) and amino (-NH_2). Chitosan can be used in the form of aerogels (Liao *et al.* 2018), magnetic particles

doi: 10.2166/wst.2020.075

(Mahfouz *et al.* 2015) and fibers (Du *et al.* 2014) for uranium adsorption to address the particle loss issues. Among these, the magnetic particles have mostly been used for their easy recycling and convenient preparation. However, the specific surface areas are not large enough for the magnetic particles to contact the uranium ions in aqueous solutions. Considering the above factors, fiber-based adsorbents are regarded as the most feasible, flexible and practical adsorbents, with the characteristics of good recyclability and high specific surface area (Wang *et al.* 2018). Electron-donating groups like carboxyl, amino (Huynh *et al.* 2017), amidoxime (Gunathilake *et al.* 2015), phosphate and phosphonate groups (Shao *et al.* 2018) have been reported to effectively improve the affinity between absorbent surface and uranyl species by modification. However, the chemical modification process is usually complicated. For fiber-based chitosan, its abundant amino and hydroxyl groups, together with its low cost, high specific surface area and renewability make it a promising adsorbent for the removal of uranium from water.

In this study, homogeneous three-dimensional fiber-network chitosan films with high mechanical strength and large surface area were prepared by dissolving in an alkali/urea system followed by regeneration from ethanol aqueous solution. This is a green route that is highly efficient, energy saving and eco-friendly. The three-dimensional fiber-network structure provides numerous active sites and the interconnected channels make it easy for the uranium solute to diffuse to the interior space of the chitosan, thus increasing the uranium adsorption capacity. The mechanism of film fabrication and uranium adsorption were also investigated.

MATERIALS AND METHODS

Materials

Chitosan (DD $\geq$ 98%, Mw $= 36.0 \times 10^4$, viscosity $= 78$ mpa.s) was purchased from Ruji Biotechnology company (Shanghai, China). Lithium hydroxide monohydrate (AR 98%), potassium hydroxide (AR 90%), and urea (AR $\geq$ 99%) were supplied by Sinopharm Chemical Reagent Co., Ltd (Beijing, China). U_3O_8 was obtained from $UO_2(NO_3)_2{\cdot}6H_2O$ by heating at 500 °C for 2 hours in a muffle furnace. Uranium stock solution was prepared by dissolving U_3O_8 (1.179 g) in a mixed solution which consisted of 10 ml concentrated nitric acid and 2 ml 30% hydrogen peroxide that was heated until the dissolved solution turned to fused salt; finally it was diluted to 1,000 mg U/L with deionized water. The standard uranium solutions were further diluted with the stock solution and the uranium concentrations were determined by the ultraviolet spectrophotometer method using arsenazo III as the chromogenic agent.

Preparation of three-dimensional fiber-network chitosan films

The alkali/urea solvent was prepared by dissolving lithium hydroxide monohydrate, potassium hydroxide, urea and deionized water at weight ratio of 8:7:8:77. Chitosan was dispersed in the alkali/urea solvent under constant stirring for 5 min and frozen at −30 °C for 6 hours. Then the frozen solution was thawed and stirred to form a homogeneous solution, and the dissolved chitosan solution of 4 wt% was obtained after centrifugation.

The preparation of chitosan films: The obtained chitosan solution was cast on a glass plate to create a film with a thickness of 0.4 mm, and then immediately immersed into coagulation solution (ethanol aqueous solutions with different concentrations) for 2 hours to form the chitosan hydrogel. The hydrogel was thoroughly washed to remove the residuals and freeze-dried to obtain the final film. The samples prepared from 0%, 20%, 40%, 50%, 70%, 80% ethanol aqueous solution were denoted as CS-0%, CS-20%, CS-40%, CS-50%, CS-70% and CS-80%, respectively.

Characterization

The structure information was detected by powder X-ray diffraction (XRD) patterns on X' Pert PRO MPD with Cu K_α radiation and 2θ range 5–80°. The sample was quenched with liquid nitrogen, the cross-section and surface structures were characterized by scanning electron microscopy (SEM) (JSM-6700F, Japan); N_2 adsorption-desorption isotherms using the Brunauer-Emmett-Teller (BET) equation (AUTOSORB-IQ-XR-C) were used to evaluate the surface pore distribution and the specific surface area, with the bath temperature at 77.35 K; X-ray photoelectron spectroscopy (XPS) (ESCALAB 250Xi) (the C-C peak was 284.8 eV) and attenuated total reflection-Fourier transform infrared (ATR-FTIR) (Bruker T27) were used to study the chemical structure. The zeta potential at the surface of the CS-80% was measured using SurPASS (Anton Paar), with 1×10^{-3} mol/L potassium chloride solution as the electrolyte; the distance between fixed membrane surfaces was 100–110 μm.

The mechanical properties of chitosan hydrogel were measured on the strength tester (BY-128A, Poosanda

Instrument Technology, China) at a speed of 3 mm/s, the 0.4 mm × 1 cm × 2 cm hydrogel samples were prepared for tension and elongation tests.

Adsorption experiments

The U(VI) adsorption experiments were carried out to examine the effect of pH, contact time and different U(VI) initial concentration. 0.05 g adsorbents were added to 100 mL uranium solution with oscillation in a shaker at room temperature. The samples were collected at time intervals and the concentration of uranium solution was determined using ultraviolet spectrophotometry by UV spectrophotometer (UV 9100A). The absorbance was measured at the wavelength of 670 nm.

The adsorption capacities (q) of chitosan films were calculated by Equation (1):

$$q = \frac{(C_0 - C_e)V}{m} \tag{1}$$

where q (mg/g) is the adsorption capacity, C_0(mg/L) is the initial concentration of U(VI) and C_e represents the U(VI) concentration under equilibrium. V(L) is the volume of U(VI) solution and m(g) is the amount of adsorbent.

The adsorption kinetics were studied for the adsorption rate and adsorption mechanism. The data were analyzed by the pseudo-first-order kinetics and pseudo-second-order kinetics models, as in Equations (2) and (3). The adsorption rate was limited by the diffusion process in the pseudo-first-order kinetic model. However, the pseudo-second-order kinetic model assumed that the control step of the adsorption rate was the chemical adsorption process.

$$\ln(q_e - q_t) = \ln q_e - \frac{k_1 t}{2.303} \tag{2}$$

$$\frac{1}{q_e - q_t} = \frac{1}{q_e} + k_2 t \tag{3}$$

where k_1(min^{-1}) and k_2(min^{-1}) are the adsorption rate constants, t (min) is the adsorption time, q_e(mg/g) and q_t(mg/g) are the adsorption capacities at equilibrium state and time t (min).

The adsorption isotherms were analyzed by the Langmuir and Freundlich sorption isotherm models.

The Langmuir isotherm model assumed that the monolayer adsorption process occurred on the equal and uniform surface. The Langmuir model is given as follows:

$$q_e = \frac{q_m b_L C_e}{1 + b_L C_e} \tag{4}$$

where q_m(mg/g) is the saturated adsorption capacity, b_L is the Langmuir constant.

The Freundlich isotherm model is established on the non-uniform surface for monolayer and multilayer adsorption, as in Equation (5):

$$q_e = K_F C_e^{\frac{1}{n_F}} \tag{5}$$

where K_F and n_F are the Freundlich constants.

RESULTS AND DISCUSSION

Material characterization

The chitosan film was prepared by the alkali/urea solvent system, and then the dissolved 4 wt% chitosan solution was cast on the glass plate with a thickness of 0.4 mm before being immersed in the coagulation solution. The sample regenerated from 80 vol% ethanol aqueous solution was denoted as CS-80%. The whole cross-section structure of CS-80% was characterized by SEM. From Figure 1(a_1) it can be seen that CS-80% was an asymmetric film. The surface directly exposed to the coagulation solution was dense. When the surface of chitosan solution was suddenly brought into contact with 80 vol% ethanol aqueous solution, the violent solvent exchange around the interface made the chitosan chains shrunk immediately, thus forming the dense surface (Sébastien *et al.* 2008). The glass-facing side (Figure 1(a_3)) was a three-dimensional fiber-network structure composed of fiber bundles with aggregated chitosan molecular chains. The fiber bundles cross-linked with each other and formed the three-dimensional fiber-network structures.

The structure of the chitosan film was significantly influenced by the concentration of coagulation. As shown in Figure 1(a_2) and 1(a_3), for the sample CS-80%, 80 vol% ethanol aqueous solution assisted in the formation of fiber bundles firstly and then the aggregated fibers connected to constitute three-dimensional fiber-like networks. The three-dimensional fiber-like network structure was interconnected and provided a large quantity of available sites for adsorption. For the sample CS-0%

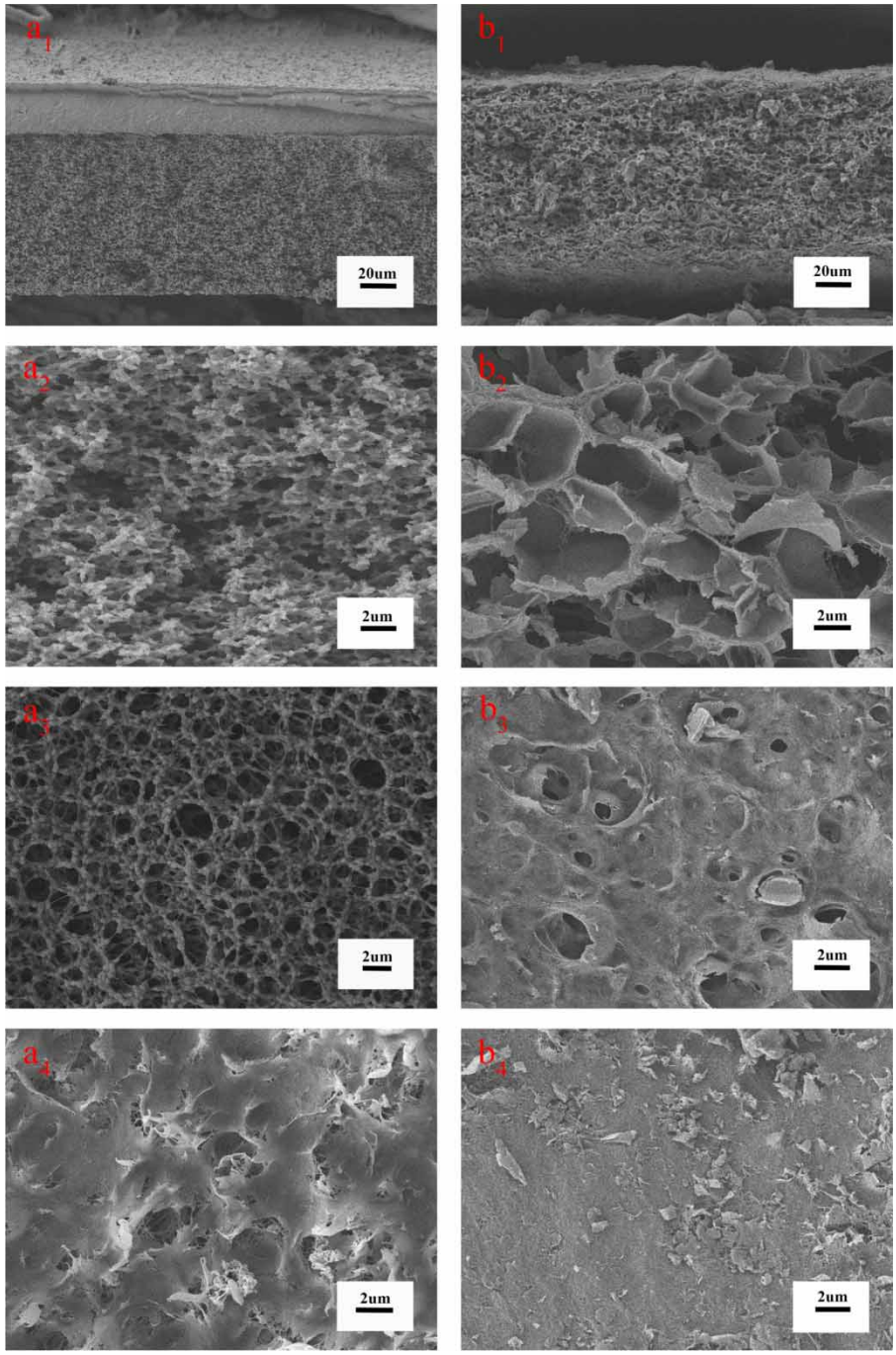

Figure 1 | SEM images of the overall cross-section morphologies of chitosan films (a_1) (b_1); the enlarged cross-section in the middle section (a_2) (b_2); the surface near the glass plate (a_3) (b_3) and the surface next to coagulation (a_4) (b_4); the symbols (a) and (b) represent the samples CS-80% and CS-0%.

which was regenerated from water, the alkali/urea solvent coalesced to form the cell-like structure shown in Figure 1(b_2). Most of those cell structures were independent of each other, leading to the block of solute in the cell-like structure during adsorption (as shown in Figure 1(b_1), 1(b_3) and 1(b_4)). For the samples of CS-20%, CS-40%, CS-50% and CS-70%, their inner structure varied from layer to layer, as shown in Figure S1 (Supplementary Material).

With the increasing concentration of ethanol, the rate of solvent exchange increased correspondingly. For the sample CS-20%, the low concentration of ethanol led to the low rate

of solvent exchange, and as a result, the alkali/urea solvent coalesced before the solvent exchange which assisted the formation of the cell-like structure. However, as the concentration of ethanol increased, as in the samples CS-40%, CS-50% and CS-70%, the increased rate of solvent exchange made the compact structure on the surface and inner part of film, although part of the film was still occupied by cell-like structure because of the concentration gradient. As for the sample CS-80%, there existed a balance between the solvent exchange and the formation of fiber bundles, thus constructing the three-dimensional fiber-like network structure.

The obvious crystalline reflection peaks marked as 110 and 130 indicated α-form chitosan, and as a result, those chitosan molecular chains were antiparallel arranged. As shown in Figure 2, the (130) lattice diffraction ($2\theta = 30^{\circ}$) of chitosan powder disappeared after the formation of chitosan hydrogel, indicating the restructuring of chitosan chains during the regeneration process. Moreover, the XRD patterns also confirmed the change of crystalline structure before and after gelation.

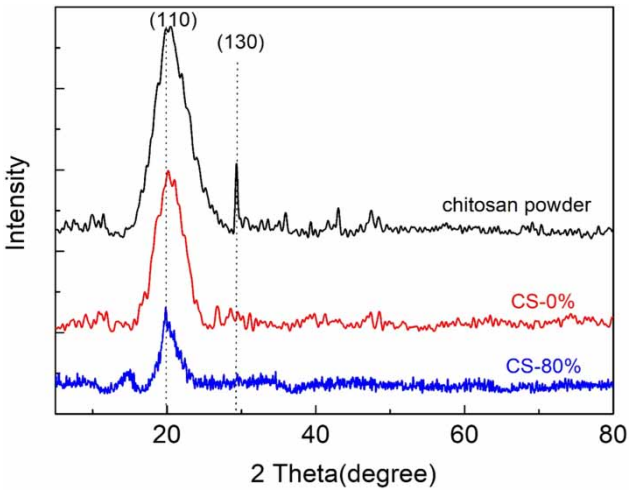

Figure 2 | XRD patterns of chitosan powder, CS-0% and CS-80%.

The hydrogels regenerated from alkali solvents, CS-0% and CS-80%, possessed better mechanical properties without any crosslinks. As shown in Figure S2 (Supplementary Material), the tensile stress of CS-0% was 1.00 MPa, with the strain of 80%, and the tensile stress of CS-80% was 0.23 MPa with the strain of 12.2%, indicating the concentration of ethanol in the coagulation solution strongly influenced the mechanical properties of chitosan hydrogels. Figure 3(a) shows the N_2 adsorption-desorption isotherms of CS-0% and CS-80%. Both of the curves were identified as type IV isotherms of mesoporous structure with H3 hysteretic loops. Moreover, the BET surface area was 12.38 m^2/g for CS-80% and 12.69 m^2/g for CS-0%; the similar BET surface area indicated that the surface area had little effect on the U(VI) adsorption.

Effect of pH

Figure 4 shows the effect of pH on U(VI) adsorption capacity in equilibrium with CS-80%. It can be seen that the pH values have an important effect on the U(VI) adsorption capacity of CS-80%, since the pH values affect not only the surface potential of the adsorbent but also the coexisting species of the complexed U(VI) ions. The U(VI) adsorption capacity increased with the increasing pH values and reached the maximum adsorption capacity at pH = 5.5. At lower pH, the complexed U(VI) ions existed mostly in the form of UO_2^{2+}; a large amount of H^+ and H_3O^+ ions would compete with UO_2^{2+}. On the other hand, the positive charge on the surface of the CS-80% adsorbents increased as

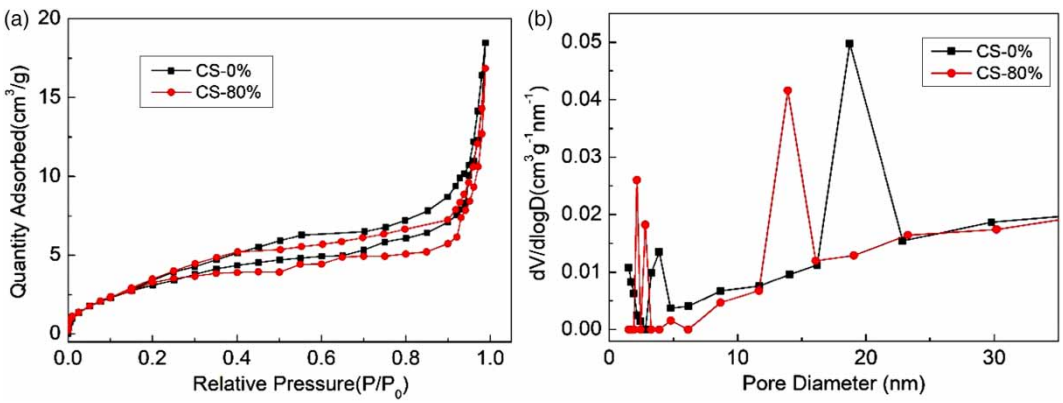

Figure 3 | (a) The N_2 adsorption-desorption isotherms of CS-0% and CS-80%; (b) the pore diameter distribution curve of CS-0% and CS-80%.

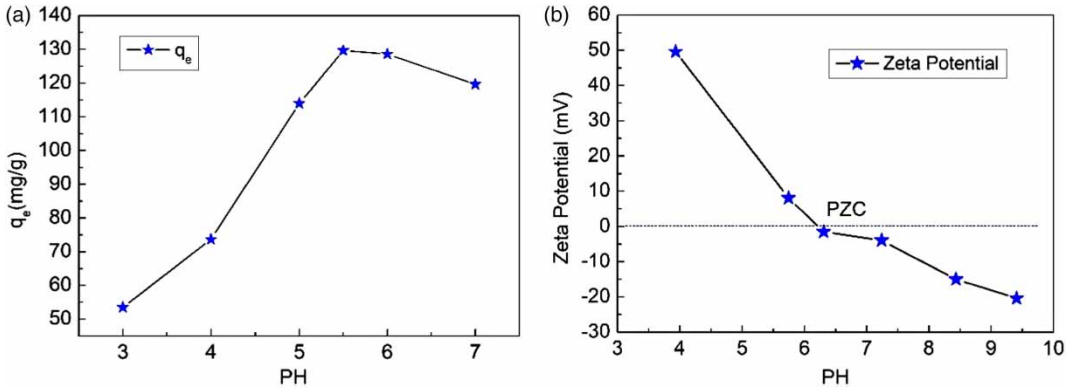

Figure 4 | (a) The effect of pH on U(VI) adsorption capacity in equilibrium with CS-80% (t = 10 hours, C_0 = 70 mg/L, V = 100 ml, T = 25 °C, SD = 0.5 g/L); (b) zeta potential at various pH values of CS-80%.

the pH decreased, as shown from the results of zeta potential (Figure 4(b)) (Wang *et al.* 2013). The electrostatic repulsion did not favor the uranium adsorption at lower pH.

With the increase in pH values, the number of competitive ions like H^+ and H_3O^+ decreased. Simultaneously, the coexisting complexed U(VI) ions like $(UO_2)_3(OH)_5^+$, $(UO_2)_4(OH)_7^+$, $(UO_2)_2(OH)_2^{2+}$ and UO_2^{2+} appeared gradually. These were beneficial to the affinity between uranium species and chitosan adsorbents. When the pH value came into the alkali range, precipitates formed, leading to a decrease of adsorption capacity (Xue *et al.* 2017). Therefore, pH = 5.0 was chosen to explore the adsorption behavior of U(VI) ions onto the sample CS-80%.

Adsorption kinetics

The effect of contact time on the U(VI) adsorption capacity of CS-80% and CS-0% is shown in Figure 5(a). The uranium adsorption was fast in the first 200 min, and increased gently after 200 min. The U(VI) adsorption capacity of CS-80% reached 114.66 mg/g at 500 min, which was significantly higher than that of CS-0% (63.51 mg/g). The higher U(VI) adsorption capacity of CS-80% was mostly associated with the interconnected three-dimensional fiber-like network structure, rather than the surface area characterized by the N_2 adsorption-desorption isotherms of CS-0% and CS-80%. The interconnected three-dimensional fiber-like network structure made the uranium aqueous solution accessible to the inner part of the CS-80% sample, and accelerated the diffuse rate simultaneously, thus resulting in a much higher adsorption capacity for CS-80% than CS-0%.

The adsorption process took place on the interface between CS-80% adsorbent and the U(VI) aqueous solution. The adsorption rate of U(VI) onto CS-80% was dominated by the interconnected fiber-like networks, which benefited the diffusion of U(VI). In addition, the large number of functional groups, such as the amine groups and hydroxyl

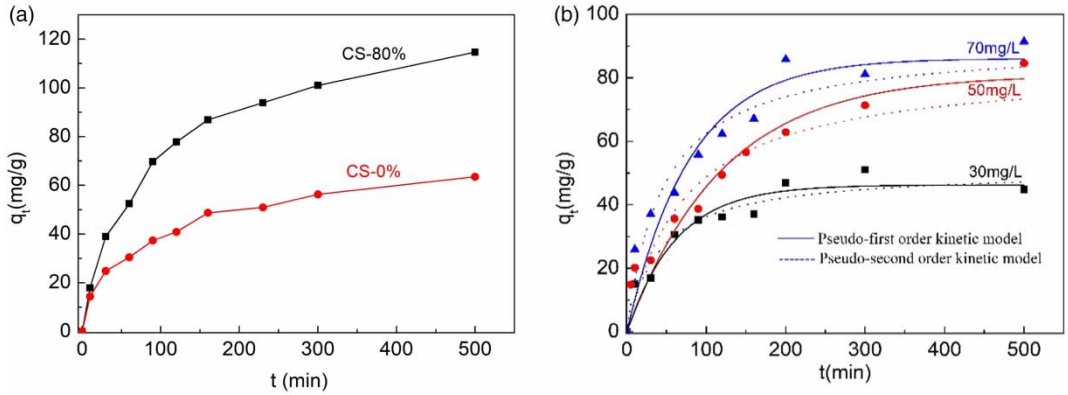

Figure 5 | (a) The effect of contact time on the U(VI) adsorption capacity of CS-0% and CS-80%; (b) the fitting of adsorption kinetic models for U(VI) with CS-80% (C_0 = 70 mg/L, pH = 5, V = 100 ml, T = 25 °C, SD = 0.5 g/L).

Table 1 | The fitting results of adsorption kinetics models

	Pseudo-first-order kinetic model			Pseudo-second-order kinetic model		
C_0 (mg/L)	q_e (mg/g)	k_1 (10^{-3} min^{-1})	R^2	q_e (mg/g)	k_2 (10^{-3} g·mg^{-1} min^{-1})	R^2
30	46.25	16.09	0.928	51	0.477	0.946
50	81.007	8.32	0.931	84	0.165	0.939
70	86.099	12.67	0.922	91	0.24	0.945

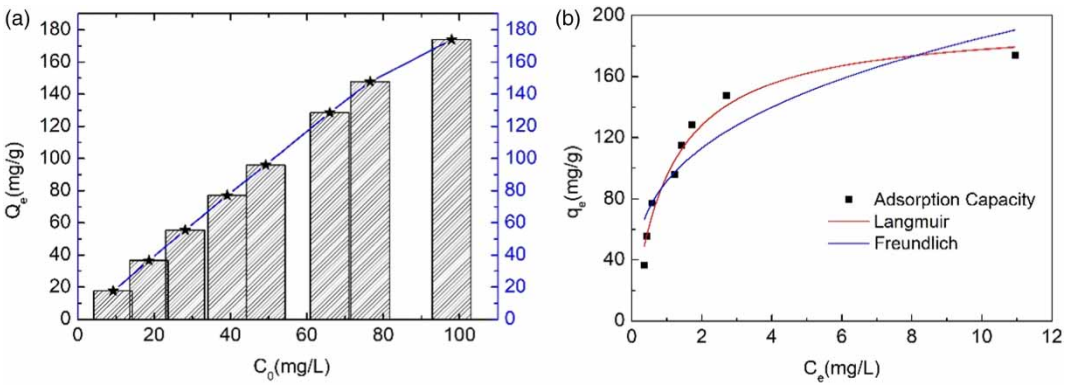

Figure 6 | (a) The effect of initial concentration on U(VI) adsorption capacity in equilibrium with CS-80%; (b) the fitting models of Langmuir and Freundlich with adsorption equilibrium (t = 10 hours, pH = 5, V = 100 ml, T = 25 °C, SD = 0.5 g/L).

Table 2 | The fitting results of adsorption isotherm models

Adsorption isotherms	Fitted model parameters	
Langmuir	q_{max} (mg/g)	196.735
	b (L/mg)	0.936
	R^2	0.967
Freundlich	K_F (mg·g^{-1}) (mg·L^{-1}) ^{n}	91.525
	N	3.264
	R^2	0.803

groups of CS-80%, also played an important role in providing strong complexed interactions with uranium ions, thus facilitating uranium adsorption.

The adsorption kinetic fitting models of U(VI) with CS-80% are shown in Figure 5(b). The results of kinetic parameters are listed on Table 1. The pseudo-first-order kinetic model and the pseudo-second-order kinetic model were used to fit the kinetic curves for investigating the adsorption mechanism. The coefficients R^2 and the adsorption capacities q_e in equilibrium of the pseudo-first-order kinetic and the pseudo-second-order kinetic models were compared. The pseudo-second-order kinetic model possessed higher related coefficients and more realistic adsorption capacity data between the experimental and the calculated values. Consequently, the pseudo-second-order kinetic model described the U(VI) adsorption kinetic model better than the pseudo-first-order kinetic model, therefore the U(VI) adsorption process was mainly controlled by chemical adsorption, and the interconnected networks structure accelerated this adsorption process.

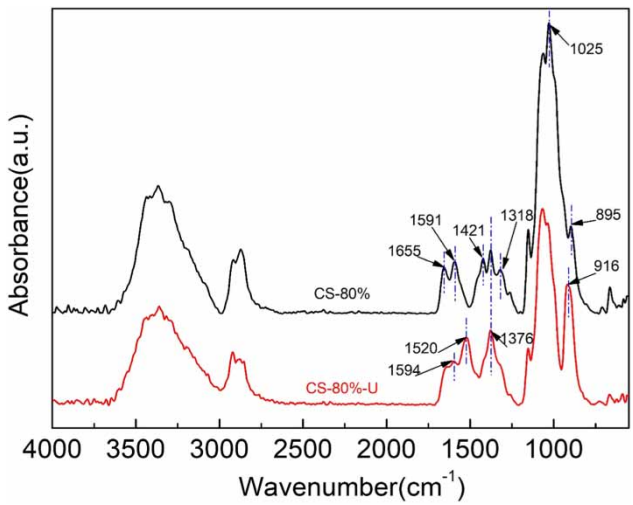

Figure 7 | ATR-FTIR spectra of CS-80% before and after U(VI) sorption.

Adsorption isotherm

The adsorption isotherm was studied to explain the adsorption mechanism of CS-80%, as shown in Figure 6(a) and 6(b). Figure 6(a) indicates that the U(VI) adsorption capacity increased with the increase of initial concentration. Figure 6(b) shows the curve between equilibrium concentration and adsorption capacity. The Langmuir model and Freundlich model were used to study the adsorption isotherm models as shown in Figure 6(b). The kinetic parameters of the Langmuir and Freundlich isotherm models are listed in Table 2. The R^2 values of the Langmuir model ($R^2 = 0.967$) is much better than the Freundlich model ($R^2 = 0.803$), indicated monolayer adsorption. This was possibly due to the homogeneous distribution of -NH_2 and -OH functional groups at the surface of the CS-80% adsorbent.

Adsorption mechanism

ATR-FTIR and XPS were used to analyze the U(VI) adsorption mechanism of CS-80%. Figure 7 shows the ATR-FTIR spectra of CS-80% and CS-80%-U (after adsorption). It can be seen that a new peak appeared at 916 cm^{-1} corresponding to the asymmetric stretching vibration of O = U = O (Piron & Domard 1998; Liao *et al.* 2018). The strength of the wide peak around 3,200–3,400 cm^{-1} associated with the combination of -OH and N-H stretching vibrations and the stretching vibration of primary -OH groups at 1,025 cm^{-1} decreased quite clearly, which indicated that the -OH groups were bound with complexed uranyl ions due to the coordination reaction. The amide III band at 1,318 cm^{-1} and the amide I band at 1,655 cm^{-1} obviously decreased after the adsorption of U(VI). Moreover, the peak at 1,591 cm^{-1} were due to the deformation vibration

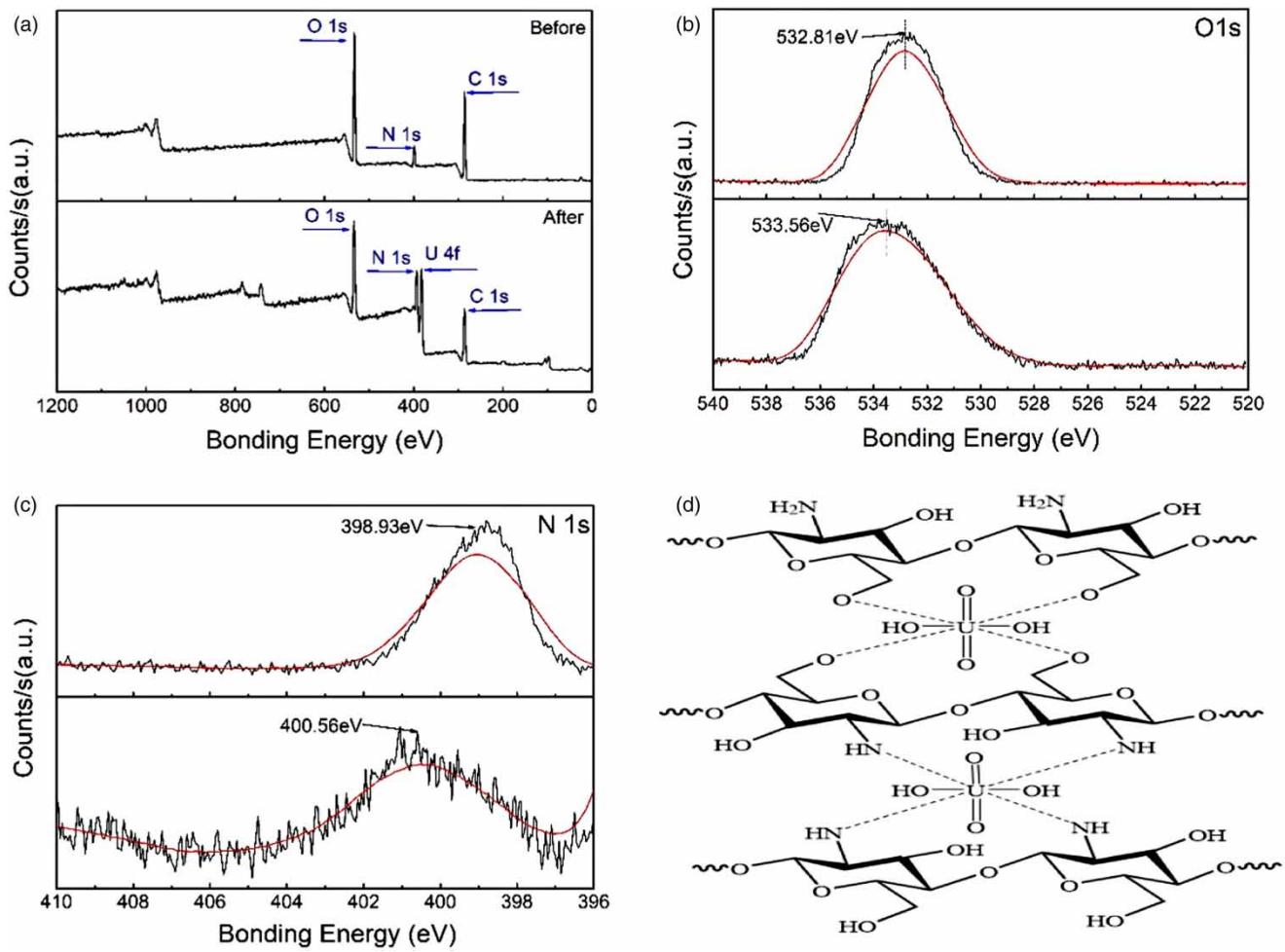

Figure 8 | XPS spectra of CS-80% before and after U(VI) sorption (a) wide scan, (b) O 1s and (c) N 1s; and (d) the adsorption mechanism of CS-80% for the complexed U(VI).

of N-H peak and the amide II band. The deformation vibration of N-H shifted to lower wavenumbers around 1,520 cm^{-1} and the amide II band clearly decreased after the adsorption of U(VI). The change of amide bands and the displacement of the deformation vibration of N-H peaks confirmed the chelation reaction between the -NH_2 groups and complexed uranyl ions (Yu *et al.* 2017).

The XPS spectra were further used to study the adsorption mechanism of U(VI) on CS-80%. As shown in Figure 8(a), the characteristic peaks of C 1s, N 1s, O 1s were identified in the spectra of CS-80% before the adsorption of U(VI). After U(VI) adsorption, the strong peaks of U 4f appeared, indicating that U(VI) was already loaded onto CS-80%. The N 1s and O 1s spectra were further characterized to analyze the functional groups which interacted with the complexed U(VI) ions. The bonding energy of N 1s shifted from 398.93 eV to 400.56 eV after the adsorption of U(VI) (Figure 8(c)). The increase of bonding energy indicated that the lone pair electrons in the outer shell of nitrogen tended to be shared with the U(VI) ions due to the chelation reaction between amine groups and the U(VI) ions. Similarly, the O 1s shift from 532.81 eV to 533.56 eV indicated that the hydroxyl group (-OH) provided lone pair electrons to the complexed U(VI) ions, which could be explained by the coordination reaction between hydroxyl groups and the U(VI) ions (Figure 8(b)).

The mechanism of uranium adsorption was attributed to the chelation reaction with the amine groups and the coordination reaction with the hydroxyl groups, as illustrated in Figure 8(d). There were mostly two hydroxyl groups (-OH) complexed with the UO_2^{2+} group, and the complexed UO_2^{2+} group would chelate with active amide groups (-NH_2) and coordinate with active -OH groups which settled at the C6 position of the glucosamine ring. Moreover, those -OH groups located on the C3 position of the glucosamine ring possibly took part in the coordination reaction with complexed UO_2^{2+} groups when those active -OH groups at the C6 position were mostly occupied.

CONCLUSIONS

The homogeneous three-dimensional fiber-network chitosan films were prepared in the alkali/urea system and used for uranium adsorption. The adsorption data fitted well with the pseudo-second-order kinetic models and the Langmuir adsorption isotherm, indicating that the process was dominated by homogeneous monolayer chemical adsorption. Due to the special interconnected fiber-network structure, the chitosan film showed the maximum adsorption capacity of 196.735 mg/g. The adsorption mechanism was attributed to chelation with -NH_2 group and coordination with -OH group on the chitosan surface, which was confirmed by ATR-FTIR and XPS. The renewable biomass and the eco-friendly preparation method provide a green strategy for developing a low-cost and high-efficiency adsorbent for the purification of uranium-containing wastewater.

ACKNOWLEDGEMENT

This work was supported by the National Nature Science Foundation of China (Grant No. 21978307 and Grant No. 21706259), the Foundation of Key Laboratory of Pulp and Paper Science and Technology of Ministry of Education/ Shandong Province of China (KF201722) and Technology Research and Development Program of Guizhou Province ([2019]2839).

SUPPLEMENTARY MATERIAL

The Supplementary Material for this paper is available online at https://dx.doi.org/10.2166/wst.2020.075.

REFERENCES

Amaral, J. C. B. S. & Morais, C. A. 2010 Thorium and uranium extraction from rare earth elements in monazite sulfuric acid liquor through solvent extraction. *Minerals Engineering* **23** (6), 498–503.

Chiramba, R., Charis, G., Fungura, N., Danha, G. & Mamvura, T. 2019 Production of activated carbon from poultry feathers for waste water treatment. *Water Science and Technology* **80** (8), 1407–1412.

Dolatyari, L., Yaftian, M. R. & Rostamnia, S. 2016 Removal of uranium(VI) ions from aqueous solutions using Schiff base functionalized SBA-15 mesoporous silica materials. *Journal of Environmental Management* **169**, 8–17.

Du, Q., Sun, J., Li, Y., Yang, X., Wang, X., Wang, Z. & Xia, L. 2014 Highly enhanced adsorption of Congo red onto graphene oxide/chitosan fibers by wet-chemical etching off silica nanoparticles. *Chemical Engineering Journal* **245**, 99–106.

Gunathilake, C., Górka, J., Dai, S. & Jaroniec, M. 2015 Amidoxime-modified mesoporous silica for uranium adsorption under seawater conditions. *Journal of Materials Chemistry A* **3** (21), 11650–9.

Huynh, J., Palacio, R., Safizadeh, F., Lefevre, G., Descostes, M., Eloy, L., Guignard, N., Rousseau, J., Royer, S., Tertre, E. & Batonneau, G. I. 2017 Adsorption of uranium over

NH_2-functionalized ordered silica in aqueous solutions. *ACS Applied Materials and Interfaces* **9** (18), 15672–15684.

Kurttio, P., Komulainen, H., Leino, A., Salonen, L., Auvinen, A. & Saha, H. 2005 Bone as a possible target of chemical toxicity of natural uranium in drinking water. *Environmental Health Perspectives* **113** (1), 68–72.

Liao, Y., Wang, M. & Chen, D. 2018 Production of three-dimensional porous polydopamine-functionalized attapulgite/chitosan aerogel for uranium(VI) adsorption. *Journal of Radioanalytical and Nuclear Chemistry* **316** (2), 635–647.

Liu, C., Hsu, P. C., Xie, J., Zhao, J., Wu, T., Wang, H., Liu, W., Zhang, J., Chu, S. & Cui, Y. 2017 A half-wave rectified alternating current electrochemical method for uranium extraction from seawater. *Nature Energy* **2** (4), 1–8.

Mahfouz, M. G., Galhoum, A. A., Gomaa, N. A., Abdel, R. S. S., Atia, A. A., Vincent, T. & Guibal, E. 2015 Uranium extraction using magnetic nano-based particles of diethylenetriamine-functionalized chitosan: equilibrium and kinetic studies. *Chemical Engineering Journal* **262**, 198–209.

Piron, E. & Domard, A. 1998 Interaction between chitosan and uranyl ions. Part 2. Mechanism of interaction. *International Journal of Biological Macromolecules* **22** (1), 33–40.

Sébastien, L., Laurent, D. & Alain, D. 2008 Multi-membrane hydrogels. *Nature* **452** (7183), 76–79.

Shao, D., Wang, X., Ren, X., Hu, S., Wen, J., Tan, Z., Xiong, J., Asiri, A. M. & Marwani, H. M. 2018 Polyamidoxime functionalized with phosphate groups by plasma technique for effective U(VI) adsorption. *Journal of Industrial and Engineering Chemistry* **67**, 380–387.

Tavakoli, H., Sepehrian, H., Semnani, F. & Samadfam, M. 2013 Recovery of uranium from UCF liquid waste by anion exchange resin CG-400: breakthrough curves, elution behavior and modeling studies. *Annals of Nuclear Energy* **54**, 149–153.

Wang, G., Wang, X., Chai, X., Liu, J. & Deng, N. 2010 Adsorption of uranium (VI) from aqueous solution on calcined and acid-activated kaolin. *Applied Clay Science* **47** (3–4), 448–451.

Wang, X., Zhu, G. & Gao, C. 2013 Adsorption of uranium(VI)on silica mesoporous material SBA-15 with short channels. *CIESC Journal* **64** (7), 2480–2487.

Wang, D., Song, J., Wen, J., Yuan, Y., Liu, Z., Lin, S., Wang, H., Wang, H., Zhao, S., Zhao, X., Fang, M., Lei, M., Li, B., Wang, N., Wang, X. & Wu, H. 2018 Significantly enhanced uranium extraction from seawater with mass produced fully amidoximated nanofiber adsorbent. *Advanced Energy Materials* **8** (33), 1802607.

Xue, G., Yurun, F., Li, M., Dezhi, G., Jie, J., Jincheng, Y., Haibin, S., Hongyu, G. & Yujun, Z. 2017 Phosphoryl functionalized mesoporous silica for uranium adsorption. *Applied Surface Science* **402**, 53–60.

Yu, R., Shi, Y., Yang, D., Liu, Y., Qu, J. & Yu, Z. Z. 2017 Graphene oxide/chitosan aerogel microspheres with honeycomb-cobweb and radially oriented microchannel structures for broad-spectrum and rapid adsorption of water contaminants. *ACS Applied Materials & Interfaces* **9** (26), 21809.

Zhou, C., Ontiveros, V. A., Cornette, S. C. L., Zevin, A. S., Carey, S. E., Krajmalnik, B. R. & Rittmann, B. E. 2014 Uranium removal and microbial community in a H_2-based membrane biofilm reactor. *Water Research* **64**, 255–264.

First received 22 November 2019; accepted in revised form 6 February 2020. Available online 19 February 2020